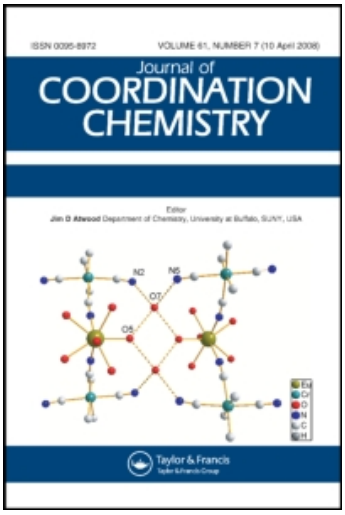

Journal of Coordination Chemistry
Publication details, including instructions for authors and subscription information:
http://www.informaworld.com/smpp/title~content=t713455674

Spectral, magnetic, thermal and electrochemical studies on new copper(II) thiosemicarbazone complexes

Gamil A. A. Al-Hazmi[a]; M. S. El-Shahawi[b]; I. M. Gabr[a]; A. A. El-Asmy[a]
[a] Chemistry Department, Faculty of Science, Mansoura University, Mansoura, Egypt [b] Chemistry Department, Faculty of Science, Mansoura University, Damietta, Egypt

To cite this Article Al-Hazmi, Gamil A. A. , El-Shahawi, M. S. , Gabr, I. M. and El-Asmy, A. A.(2005) 'Spectral, magnetic, thermal and electrochemical studies on new copper(II) thiosemicarbazone complexes', Journal of Coordination Chemistry, 58: 8, 713 — 733
To link to this Article: DOI: 10.1080/00958970500092834
URL: http://dx.doi.org/10.1080/00958970500092834

Journal of Coordination Chemistry
Vol. 58, No. 8, 20 May 2005, 713–733

Taylor & Francis
Taylor & Francis Group

Spectral, magnetic, thermal and electrochemical studies on new copper(II) thiosemicarbazone complexes

GAMIL A. A. AL-HAZMI†, M. S. EL-SHAHAWI‡,
I. M. GABR† and A. A. EL-ASMY*†

†Chemistry Department, Faculty of Science, Mansoura University, Mansoura, Egypt
‡Chemistry Department, Faculty of Science, Mansoura University, Damietta, Egypt

(*Received 19 July 2004; revised 22 September 2004; in final form 28 February 2005*)

The chelation behavior of some =N(1) and NH(4) thiosemicarbazones towards copper(II) ions has been investigated. The isolated complexes are characterized by elemental analysis, magnetic moment, electronic, IR, ESR and ms spectra, and by thermal and voltammetric measurements. The substituents on =N(1) and/or NH(4) thiosemicarbazones and the log K values of the ligands play an important role in complex formation. The IR spectra showed that the reagents HAT, HAET, HAPT, HA*p*ClPT, H_2ST and HBT are deprotonated in the complexes and act as mononegative SN donors; H_2SET, H_2S*p*ClPT, H_2HyMBPT and H_2HyMB*p*ClPT, as binegative NSO donors while H_2SPT is a mononegative NSO donor. The ESR spectra of the complexes are quite similar and exhibit axially symmetric g-tensor parameters with $g_{\parallel} > g_{\perp} > 2.0023$. The loss of thiol and/or hydroxyl hydrogen was confirmed from potentiometric titrations of the ligands and their copper(II) complexes. The protonation constants of the ligands as well as the stability constants of their Cu(II) complexes were calculated. Thermogravimetric analysis of the complexes suggests different decomposition steps. The Coats–Redfern and Horowitz–Metzger equations have been used to calculate the kinetic and thermodynamic parameters for the different thermal decomposition steps of some complexes. The redox properties, nature of the electroactive species and the stability of the complexes towards oxidation are strongly dependent on the substituents on the precursor NH(4) thiosemicarbazone. The redox data are discussed in terms of the kinetic parameters and the reaction mechanism.

Keywords: Copper(II) complexes; Thiosemicarbazones; Spectra; Thermal; Redox behavior

1. Introduction

Thiosemicarbazones have remarkable properties and have been the subject of numerous coordination chemical studies [1]. They have anticarcinogenic and antimicrobial activities [2, 3]. The fungicidal activity of these compounds is due to their ability to form stable chelates with essential metal ions, which the fungus needs in its

*Corresponding author. Email: aelasmy@yahoo.com

Journal of Coordination Chemistry
ISSN 0095-8972 print: ISSN 1029-0389 online
DOI: 10.1080/00958970500092834

metabolism [4]. In addition, some mono- or polynuclear Schiff-base copper(II) complexes based on thiosemicarbazone serve as models for enzymes such as galectose oxidase and may be used as effective oxidants and redox catalysts [5, 6]. Copper(II) complexes of salicylaldehyde [7, 8], 2-hydroxyacetophenone, 2-aminoaceto-phenone [9] and 2-acetylpyridine [10] NH(4)-substituted thiosemicarbazones have been extensively studied. The redox behavior of copper(II) model compounds is of special interest since the metal is involved in electron-transfer processes in some biological systems [5, 6]. Thus, the work reported herein is focused on the synthesis, spectroscopic and electrochemical characterization of copper(II) complexes of this class of ligands. The electrochemical behavior of some of these complexes was investigated by cyclic voltammetry because of their possible applications as superoxide dismutase mimetic complexes and as copper sensors. In addition, the decomposition kinetics and thermodynamic characteristics of the decomposition steps of some of the complexes have been studied employing Coats–Redfern and Horowitz–Metzger equations.

2. Experimental

All chemicals used were of analytical reagent grade (BDH) and were used as supplied. The formulae, abbreviations and the names of the ligands are listed in table 1. Tetrabutylammonium tetrafluoroborate ($TBA^+BF_4^-$) was used as a supporting electrolyte.

2.1. *Synthesis of ligands*

The thiosemicarbazones, figure 1, (see table 1 for full and abbreviated names) were prepared as reported earlier [11] by condensing 1:1 molar ratios of acetophenone, salicylaldehyde, benzophenone or 2-hydroxy-4-methoxybenzophenone in ethanol with ethanolic solutions of some nitrogen compounds, thiosemicarbazide, ethyl-, phenyl- or *p*-chlorophenyl-thiosemicarbazides. The reaction mixtures were refluxed in a water bath for 2–3 h in the presence of few drops of glacial acetic acid. The formed precipitates were separated by filtration, recrystallized from ethanol and dried. The proposed formulae of the ligands are in good agreement with the stoichiometries concluded from their analytical data and mass spectra and confirmed from the IR spectral data (table 3). The ^{1}H NMR spectra of HAET, HAPT and H_2HyMPT in d_6-DMSO showed signals at δ 12.08–11.40 and 9.92–8.51 assigned to the NH(2) and NH(4) protons, respectively [12]. The spectra of HAT and H_2ST showed signals at δ 10.29, 10.07 and 8.09, 8.03 assigned to the NH(2) and NH_2 protons, respectively. Moreover, the spectrum of H_2ST showed the OH proton signal at 10.17 ppm [13].

2.2. *Synthesis of copper(II) complexes*

The complexes were prepared by refluxing a 1:1 molar mixture of each ligand (3 mmol) with copper acetate (3 mmol). The reaction mixture was refluxed on a water bath for 4–6 h. The precipitate was filtered off, washed with hot water, hot ethanol and diethyl ether and finally dried in a vacuum desiccator over anhydrous $CaCl_2$.

Table 1. Abbreviated and full names, melting points, elemental analyses and formulas weights (FW) of the ligands.

Abbreviated name	Full name	Color	M.P., °C	Found (Calcd. %)		FW	
				C	H	Found*	Calcd.
HAT	1-Acetophenonethiosemicarbazone	White	132	55.8 (55.9)	5.7 (5.7)	–	193.3
HAET	1-Acetophenone-4-ethylthiosemicarbazone	White	145	60.0 (59.7)	6.4 (6.8)	221.0	221.3
HAPT	1-Actophenone-4-phenylthiosemicarbazone	White	198	67.0 (66.9)	5.9 (5.6)	–	269.4
HA*p*ClPT	1-Acetophenone-4-*p*-chlorophenylthiosemicarbazone	Yellowish white	190	58.8 (59.3)	4.2 (4.6)	304.0	303.8
H_2ST	1-Salicylaldehydethiosemicarbazone	Yellow	245	49.3 (49.2)	5.0 (4.6)	–	195.2
H_2SET	1-Salicylaldehyde-4-ethylthiosemicarbazone	White	184	53.3 (53.8)	5.4 (5.9)	223.0	223.3
H_2SPT	1-Salicylaldehyde-4-phenylthiosemicarbazone	Yellowish white	205	61.0 (61.9)	4.8 (4.8)	–	271.3
H_2S*p*ClPT	1-Salicylaldehyde-4-*p*-chlorophenylthiosemicarbazone	Yellow	212	54.3 (54.9)	4.0 (3.9)	304.0	305.9
H_2HyMBPT	1-(2-Hydroxy-4-methoxybenzophenone) 4-phenylthio-semicarbazone	Yellow	110	66.0 (66.8)	4.8 (5.1)	377.0	377.5
H_2HyMB*p*ClPT	1-(2-Hydroxy-4-methoxybenzophenone) 4-*p*-chloro-phenylthiosemicarbazone	Yellow	135	61.2 (61.2)	4.3 (4.4)	412.0	411.9
HBT	1-Benzophenonethiosimecarbazone	White	191	66.6 (65.8)	4.6 (5.1)	255.9	255.3

*Values obtained from mass spectra.

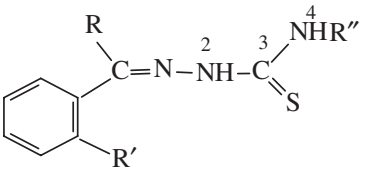

R = H or CH_3
R′ = H or OH
R″ = H, C_2H_5, C_6H_5 or p-ClC_6H_4

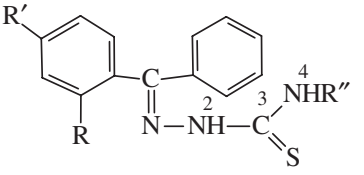

R = H or OH
R′ = H or OCH_3
R″ = H, C_6H_5 or p-ClC_6H_4

Figure 1. Chemical formulae of the thiosemicarbazone ligands.

2.3. *Chemical and physical measurements*

Carbon and H contents were determined at the Microanalytical Unit of Cairo University. Copper analysis was carried out according to the standard method [14]. The infrared spectra (KBr discs), electronic spectra (Nujol mulls and DMF solutions), ^{1}H NMR in d_6-DMSO (200 MHz) and mass spectra were recorded on a Mattson 5000 FTIR spectrophotometer, UV_2 Unicam UV/Vis, Varian Gemini and Varian MAT 311 spectrometers, respectively. Magnetic moment values were evaluated at room temperature ($25 \pm 1^\circ$C) using a Johnson Matthey magnetic susceptibility balance. ESR spectra were obtained on a Bruker EMX Spectrometer working in the X-band (9.78 GHz) with 100 kHz modulation frequency. The microwave power and the modulation amplitude were set at 1 mW and 4 Gauss, respectively. The low-field signal was obtained after four scans with a tenfold increase in receiver gain. Powder ESR spectra were obtained in 2 mm quartz capillaries at room temperature. Thermal studies were carried out on a Shimadzu thermogravimetric analyzer at a heating rate of 10°C min^{-1} under nitrogen. Cyclic voltammetry measurements were carried out with a Potentiostat wave generator (Oxford Press) equipped with a Phillips PM 8043 X–Y recorder. The electrochemical cell assembly consisted of platinum wires of 0.5 mm diameter as working and counter electrodes and Ag/AgCl as a reference electrode. The protonation constants of the ligands and the formation constants of their complexes at 298.05 K were determined potentiometrically by the Irving–Rossotti method [15].

3. Results and discussion

The formulae of the complexes are listed in table 2 together with their physical properties, elemental analyses and formula weights obtained from mass spectra. The isolated solid complexes are stable at room temperature, non-hygroscopic in nature and almost insoluble in water and in most organic solvents but are very soluble in DMF and DMSO. Most decomposed on heating at $> 300^\circ$C.

3.1. *IR spectral studies*

The most important infrared bands of the ligands and their copper(II) complexes with their probable assignments are given in table 3. The existence of numerous

Table 2. Physical properties, analytical data and formula weights (FW) of the copper(II) complexes.

No.	Complex	Color	M.P., °C	Found (Calcd. %)			FW	
				C	H	Cu	Found*	Calcd.
1	$[Cu(AT)(OH)(H_2O)_3]$	Olive green	> 300	33.0 (33.1)	4.8 (5.2)	19.3 (19.4)	327.0	326.8
2	$[Cu(AET)(OH)(H_2O)]$	Brown	> 300	41.0 (41.4)	5.2 (5.4)	19.5 (19.9)	321.0	318.9
3	$[Cu_2(APT)_3(OAc)]$	Olive green	200	56.1 (56.9)	4.5 (4.6)	12.8 (12.8)	–	991.2
4	$[Cu(ApClPT)(OAc)(C_2H_5OH)]$	Green	> 300	47.9 (48.4)	4.5 (4.7)	13.5 (13.5)	470.0	471.5
5	$[Cu(HST)_2\ ]\cdot H_2O$	Dark brown	> 300	40.5 (40.9)	3.9 (3.8)	13.4 (13.5)	468.3	470.0
6	$[Cu_2(SET)(Oac)_2(H_2O)_2]\cdot H_2O$	Brown	248	32.0 (32.3)	4.3 (4.6)	24.0 (24.4)	519.2	520.5
7	$[[Cu(HSPT)(OAc)(H_2O)_2]\cdot H_2O$	Yellowish green	> 300	42.4 (43.0)	4.4 (4.7)	13.8 (14.2)	–	446.9
8	$[Cu_2(SpClPT)(OH)_2(H_2O)_2]$	Yellowish brown	> 300	32.8 (33.6)	3.5 (3.2)	25.4 (25.4)	500.7	500.9
9	$[Cu(HyMBPT)(H_2O)_3]\cdot 0.5H_2O$	Olive green	> 300	49.4 (50.2)	4.6 (4.8)	12.8 (12.6)	502.5	502.0
10	$[Cu(HyMBpClPT)(H_2O)]$	Greenish brown	> 300	50.8 (51.3)	3.4 (3.7)	13.5 (12.9)	491.2	491.4
11	$[Cu_2(BT)(OAc)(OH)_2(H_2O)]\cdot H_2O$	Olive green	> 300	38.0 (37.6)	4.3 (4.1)	25.2 (24.9)	508.0	510.5

*Values obtained from mass spectra.

Table 3. Most significant most IR spectral data (cm^{-1})[a] of the copper(II) complexes and corresponding bands of the free ligands in parentheses.

Complex	ν (NH_2)	ν (OH)	ν (N^4H)	ν (N^2H)	ν (C=N)	ν (C=S)	ν (C–S)	δ(OH)	ν (Cu–O)	ν (Cu–N)	ν (Cu–S)
1	3380, sh (3410, s) 3335, w (3370, w)	3415, m	–	(3220, w)	1590, s (1630, s)	(790, m)	615, m	1345, w	–	445, w	370, w
2	–	3570, vs	3260, sh (3320, s)	(3225, s)	1565, m (1630, m)	(790, m)	615, s	1345, m	495, m	445, w	365, w
3	–	–	3325, s, br (3300, m)	(3250, m)	1590, m (1605, m)	(795, m)	615, w	–	500, w	410, w	340, w
4	–	–	3290, w (3290, s)	(3240, m)	1625, w (1635, w)	(795, m)	690, w	–	500, w	445, w	350, w
5	3365, w (3370, w) 3275, w (3315, s)	3440, w (3440, w)	–	(3165, m)	1595, s (1610, s)	(780, w)	630, w	1365, s (1365, s)	–	430, w	340, w
6	–	(3405, w)	3355, m, br (3355, s)	(3250, s)	1600, vs (1605, m)	(790, m)	640, w	(1375, m)	485, w	400, w	330, w
7	–	3405, w (3405, w)	3345, m, br (3380, w)	(3145, m)	1600, vs (1620, s)	(835, w)	650, w	1370, m (1389, m)	500, m	430, w	355, w
8	–	3350, m, br (3335, m)	3225, sh (3235, m)	(3154, m)	1600, vs (1610, s)	(830, w)	610, w	1315, s (1330, m)	500, w	440, w	355, w
9	–	(3470, w)	3280, w (3300, s)	(3160, m)	1595, m (1635, m)	(810, w)	660, w	(1325, m)	490, w	425, w	365, w
10	–	(3440, w)	3280, m (3290, s)	(3180, s)	1625, m (1635, s)	(790, w)	615, w	1315, m (1350, m)	495, w	430, w	340, w
11	3340, w (3365, m) 3265, w (3260, m)	3410, w	–	(3175, s)	1600, m (1620, m)	(800, m)	610, w	1380, s	470, w	425, w	340, w

[a]s = Strong, m = medium, w = weak, v = very, br = broad and sh = shoulder.

coordination sites in the ligands gives variable bonding modes. Comparison of the IR spectra of ligands and their copper(II) complexes revealed that the ligands are bonded to the Cu(II) ions in their thiol form with several coordination modes. In the complexes $[Cu(AT)(OH)(H_2O)_3]$ (**1**), $[Cu(AET)(OH)(H_2O)]$ (**2**), $[Cu_2(APT)_3(OAc)]$ (**3**), $[Cu(ApClPT)(OAc)(C_2H_5OH)]$ (**4**), $[Cu(HST)_2]\cdot H_2O$ (**5**) and $[Cu_2(BT)(OAc)(OH)_2(H_2O)]\cdot H_2O$ (**11**), the ligands are mononegative, bidentate, and the spectra prove that the =N and S atoms are the coordination centers. Strong evidence arises from: (i) the disappearance of $\nu(N^2H)$; (ii) the negative shift (10–65 cm^{-1}) of ν(C=N) [16]; (iii) the appearance of a new band, attributed to $\nu(C{=}N^*)$, at the same position as for the ν(C=N) of the thiosemicarbazone; (iv) coordination of the azomethine nitrogen is also consistent with the presence of a new band at 410–445 cm^{-1} assignable to the ν(Cu–N) vibration [17] and finally (v) coordination *via* thiolate sulfur is indicated by the absence of the characteristic thioamide ν(C=S) vibration with the simultaneous appearance of new bands in the regions 610–690 and 325–370 cm^{-1} due to ν(C–S) and ν(Cu–S) vibrations [17, 18], respectively. In the complexes $[Cu_2(SET)(OAc)_2(H_2O)_2]\cdot H_2O$ (**6**), $[Cu_2(SpClPT)(OH)_2(H_2O)_2]$ (**8**), $[Cu(HyMBPT)(H_2O)_3]\cdot 0.5\,H_2O$ (**9**) and $[Cu(HyMBpClPT)(H_2O)]$ (**10**), the ligands are binegative, tridentate, and interact with the Cu(II) ions via N (azomethine), S and phenolic oxygen atoms by releasing the hydrogen ions from both thioamide, through thioenolization, and OH groups. This mode of chelation was confirmed by: (i) the disappearance of $\nu(N^2H)$ and ν(C=S) conjugated with the appearance of ν(C–S) at 610–640 cm^{-1} and ν(Cu–S) at 330–365 cm^{-1}; (ii) the phenolate group acts as the third coordination site to the metal ion indicated by disappearance of the stretching [ν(OH)] and bending [δ(OH)] vibrations; (iii) the band arising from ν(C=N) in the free ligand is shifted (10–40 cm^{-1}) upon coordination towards a lower frequency region in the complex spectra and finally (iv) the observation of new bands in the regions 485–500 and 400–425 cm^{-1} attributed to ν(Cu–O) [18] and ν(Cu–N) vibrations, respectively, confirming bonding through oxygen and nitrogen. In the complex $[Cu(HSPT)(OAc)(H_2O)_2]\cdot H_2O$ (**7**), the ligand is mononegative, tridentate by deprotonation of the thioamide (NHCS) group upon thioenolization and coordination to copper(II) through the C=N, OH and C–S groups. The shift to lower frequency (15 cm^{-1}) of the ν(OH) vibration lends support OH participation. Thioenolization is confirmed by the disappearance of ν(C=S) and $\nu(N^2H)$ with the appearance of ν(C–S) at 650 and ν(Cu–S) at 355 cm^{-1}. Also, the new band observed at 500 cm^{-1} assigned to ν(Cu–O) provides additional support for oxygen donation from the hydroxyl group. The bands due to ν(C=N) are shifted to lower frequency in the spectrum of the complex with the appearance of a new band at 430 cm^{-1} assignable to ν(Cu–N). All the data support the mononegative tridentate (SNO) behavior of H_2SPT (figure 2).

In the complexes, $[Cu(ApClPT)(OAc)(C_2H_5OH)]$ (**4**), $[Cu_2(SET)(OAc)_2(H_2O)_2]\cdot H_2O$ (**6**) and $[Cu(HSPT)(OAc)(H_2O)_2]\cdot H_2O$ (**7**), the acetate group coordinates in a monodentate manner as indicated by the frequency difference ($\Delta\nu \geq 190\,cm^{-1}$) between ν_s and ν_{as} vibrations [19, 20] whereas, in the complexes $[Cu_2(APT)_3(OAc)]$ (**3**) and $[Cu_2(BT)(OAc)(OH)_2(H_2O)]\cdot H_2O$ (**11**), the acetate group coordinates to the copper(II) ions in a bridging bidentate fashion as indicated by the difference ($\Delta\nu \leq 180\,cm^{-1}$) between the two acetate bands. Finally, the bands

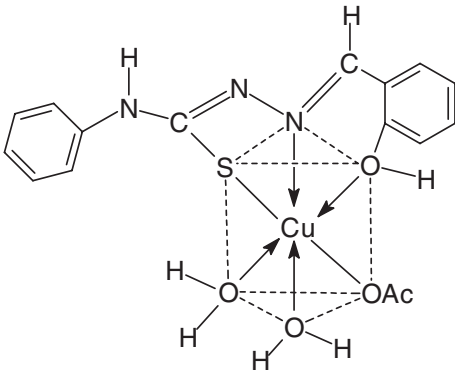

Figure 2. The proposed structure of $[Cu(HSPT)(OAc)(H_2O)_2]\cdot H_2O$ (**7**).

Table 4. Formation constants of the complexes and deprotonation constants of ligands (in parentheses).

	Half method				Least-squares method			
System	log K_1	Log K_2	log K_3	log β	log K_1	log K_2	log K_3	log β
Cu(II)–HAT	9.87 (11.29)	4.29	–	14.16	9.85 (11.30)	4.29	–	14.14
Cu(II)–HAET	9.33 (9.88)	4.74	–	14.07	9.40 (9.88)	4.75	–	14.15
Cu(II)–HAPT	6.42 (6.47)	5.92	4.50	16.84	(6.46)	5.70	4.55	10.25
Cu(II)–A*p*ClPT	(8.72)	8.53	6.10	14.63	(8.65)	8.42	–	8.42
Cu(II)–H_2ST	13.71 (12.39)	7.82 (10.00)	–	21.53	13.83 (12.36)	7.91 (10.00)	–	21.74
Cu(II)–H_2SET	15.31 (10.80)	5.94 (6.00)	–	21.25	15.35 (10.80)	6.20 (6.10)	–	21.55
Cu(II)–H_2SPT	(10.25)	7.96 (7.92)	–	7.96	13.21 (10.24)	8.10 (7.79)		21.31
Cu(II)–H_2S*p*ClPT	(11.29)	7.25 (8.32)	–	7.25	(11.30)	7.30 (8.30)	–	7.30
Cu(II)–H_2HyMBPT	13.08 (11.48)	8.08 (4.82)	–	21.16	13.00 (11.48)	8.10 (4.92)	–	21.10
Cu(II)–H_2HyMB*p*ClPT	(11.36)	8.13 (9.27)	–	8.13	(11.42)	8.15 (9.35)	–	8.15
Cu(II)–HBT	10.38 (11.20)	–	–	10.38	10.40 (11.00)	–	–	10.40

log β = Overall formation constant.

of coordinated water observed at 810–860 and 530–595 cm^{-1}, are assigned to $\rho_r(H_2O)$ and $\rho_w(H_2O)$, respectively [21].

Strong evidence for the loss of hydrogen ion(s) is supported by the potentiometric studies.

3.2. *Potentiometric studies*

Potentiometric (pH-metric) titrations of the ligands and their copper(II) complexes against 0.01 M NaOH, in the absence or in the presence of HCl (0.01 M) in ethanol–water (50% v/v) at $\mu = 0.1$ M were carried out [22]. The values of the average number of protons (n_A^-), the average number of ligand molecules attached per metal ion (n^-) and the free ligand exponent (pL) were calculated at different pH values. Plotting of (n_A^-) versus pH gives the proton-ligand formation constant (log K_1 and/or log K_2). The data calculated from the half- and least-square methods [15] are summarized in table 4. The log K values of the investigated

ligands depend not only on the chemical structure but also on the inductive effect of the substituents. Careful inspection of the data (table 4) reveals that:

(a) The following observations may be considered concerning the substituents on the N^4H group: (i) the ligands containing NH_2 group (R″ H in figure 1) have high log K_1 values which decrease, for each category, in the following order: H > Et > *p*ClPh > Ph; (ii) the presence of H or Et (electron-donating) increases the electron density on the azomethine group which hinders the deprotonation and increases the basicity of the ligands and (iii) the presence of an electron-withdrawing group (Ph or *p*ClPh) decreases the electron density on the azomethine moiety and enhances deprotonation. Thus, the latter ligands are less basic (lower log *K*) than the former ones.
(b) The substituents on the C=N group have a great effect on the basicity of the ligands. The order of the ligands is: H_2ST > HAT > HBT. The two phenyl groups of the benzophenone moiety decrease the electron density on the azomethine group facilitating proton withdrawal by the inductive effect.

The metal–ligand stability constants were determined by applying the curve-fitting method to the data of n^- versus *p*L and the results are summarized in table 4. The data revealed that the values of log K_1 are higher than those of log K_2 or log K_3 for the same complex because all available sites for binding the first ligand are free which is not the case for binding the second or third. According to the values of log K_1 + log K_2, the stability of the complexes varied with the substituents on the thiosemicarbazone moiety in the following sequence for the ligands:

$$H_2SET > H_2ST > H_2HyMBPT > HBT > HAT > HAET > HAPT$$

The bulky 2-hydroxy-4-methoxybenzophenone decreases the stability of its complex more than the salicylaldehyde moiety. Also, the increase in the volume of the NH(4) substituents showed the same trend of stability, H > Et > Ph.

3.3. *Electronic spectra and magnetic studies*

The magnetic moments and the significant electronic absorption bands of the copper(II) complexes, recorded in DMF solution and in Nujol mull, are given in table 5. Thiosemicarbazones have a ring $\pi \rightarrow \pi^*$ band at 32 785–40 815 cm^{-1} and $n \rightarrow \pi^*$ band at 28 570–30 960 cm^{-1} [17]; little change in their energies are recorded for their complexes. Another $n \rightarrow \pi^*$ band in the spectra of the free thiosemicarbazones is also found in the spectra of the copper(II) complexes at 27 000–28 250 cm^{-1}.

The band at 22,220–26,040 cm^{-1} in the spectra (DMF) of the complexes may be due to LMCT [23]. Previous studies on copper(II)-thiosemicarbazones indicated that a band in the region 25 000–26 040 cm^{-1} could be assigned to an O → Cu(II) transition [24] whereas a band in the range 21 785–24 750 cm^{-1} is due to a S → Cu(II) transition [25]. The CT band of the complexes is therefore due to S → Cu CT owing to the greater reducibility of copper(II) in the presence of sulfur compounds than with oxygen compounds.

The electronic spectra of $[Cu(AT)(OH)(H_2O)_3]$ (**1**), $[Cu(HSPT)(OAc)\text{-}(H_2O)_2] \cdot H_2O$ (**7**) and $[Cu(HyMBPT)(H_2O)_3] \cdot 0.5\,H_2O$ (**9**) in Nujol and DMF are similar indicating

Table 5. Magnetic moments, electronic spectra (cm^{-1}) in DMF (Nujol) and ESR data for the copper(II) complexes.

Complex	μ_{eff} (BM)	d–d Transition bands	Charge-transfer bands	Spin Hamiltonian parameters					
				$g_{\parallel}$	$g_{\perp}$	$A_{\parallel} \times 10^{-4}$ (cm^{-1})	G	α^2	β^2
1	2.20	13 335 (14 285)	23 210 (23 200)	2.38	2.06	170	6.30	0.91	0.89
2	1.90	17 480 (17 545)	24 440 (22 575)	–	–	–	–	–	–
3	1.72	17 450 (20 000)	22 470 (21 980)	2.15	2.04	165	3.75	0.66	0.67
4	2.32	16 665 (16 975)	22 220 (22 470)	–	–	–	–	–	–
5	1.53	16 805 (17 230)	25 380 (22 505)	2.27	2.08	160	3.37	0.78	0.89
6	1.86	17 095 (17 100)	25 000 (22 125)	–	–	–	–	–	–
7	2.06	15 600 (14 245)	24 750 (25 510)	–	–	–	–	–	–
8	1.48	17 480 (17 795)	24 690	–	–	–	–	–	–
9	1.80	13 175 (14 365)	23 750 (24 510)	–	–	–	–	–	–
10	1.91	12 880 (18 115)	26 040 (21 785)	–	–	–	–	–	–
11	1.20	16 585 (15 890)	–	–	–	–	–	–	–

that DMF has no effect on complex formation. The broad band centered at 13 175–15 600 cm^{-1} (DMF) and ≈14 300 cm^{-1} (Nujol) is assigned to the $^2E_{2g} \rightarrow {}^2T_{2g}$ transition in an octahedral geometry [25]. The broadness of the observed band may be due to the Jahn–Teller effect, which enhances the distortion of the octahedral geometry. The green color of these complexes supports the proposed geometry. The magnetic-moment values were found within the range reported for d^9 systems containing one unpaired electron and suggest Cu–L covalent bonds.

The electronic spectra of [Cu(AET)(OH)(H_2O)] (**2**), [Cu_2(APT)$_3$(OAc)] (**3**), [Cu(A*p*ClPT)(OAc)(C_2H_5OH)] (**4**), [Cu_2(SET)(OAc)$_2$(H_2O)$_2$]·H_2O (**6**) and [Cu_2(BT)(OAc)(OH)$_2$(H_2O)]·H_2O (**11**) show one band at 15 890–20 000 cm^{-1} (Nujol) and 16 585–17 480 cm^{-1} (DMF), indicating a square-planar geometry. For square-planar complexes, three spin-allowed transitions are possible, assigned to $^2B_1 \rightarrow {}^2A_1$ $\nu_1(d_{x^2-y^2} \rightarrow d_{z^2})$, $^2B_1 \rightarrow {}^2B_2\,\nu_2(d_{x^2-y^2} \rightarrow d_{xy})$ and $^2B_1 \rightarrow {}^2E\,\nu_3(d_{x^2-y^2} \rightarrow d_{xz}, d_{yz})$ but the band could not be resolved into three bands [26]. This geometry is further supported by the values of their magnetic moments [26]. The lowest value (1.20 BM) for [Cu_2(BT)(OAc)(OH)$_2$(H_2O)]·H_2O (**11**) indicates a significant interaction between the copper(II) centers [27]. Moreover, the complex [Cu(A*p*ClPT)(OAc)(C_2H_5OH)] (**4**) has a magnetic moment (2.32 BM) higher than the calculated value for one unpaired electron and may be due to spin-orbit coupling [27].

The electronic spectra of the complexes [Cu(HST)$_2$]·H_2O (**5**), [Cu_2(S*p*ClPT)(OH)$_2$(H_2O)$_2$] (**8**) and [Cu(HyMB*p*ClPT)(H_2O)] (**10**) show a band at 17,230–18 115 cm^{-1} (Nujol) and 12 880–17 480 cm^{-1} (DMF), which is safely assigned to the $^2T_2 \rightarrow {}^2E$ transition in a tetrahedral symmetry [28]. The magnetic moments (table 5) of the complexes [Cu(HST)$_2$]·H_2O (**5**) and [Cu_2(S*p*ClPT)(OH)$_2$(H_2O)$_2$] (**8**) are below the expected value (1.70–2.20 BM) for a tetrahedral geometry which may be attributed to copper–copper interaction [29].

The band positions in the spectrum of [Cu(HyMB*p*ClPT)(H_2O)] (**10**) in DMF are very different from that recorded in Nujol (table 5) showing that the complex is significantly affected by solvolysis or hydrogen bonding. In DMF solution, some complexes have d–d transitions larger or smaller (table 5) than those recorded for solid complexes suggesting that the same species are present both in the solids and the solutions.

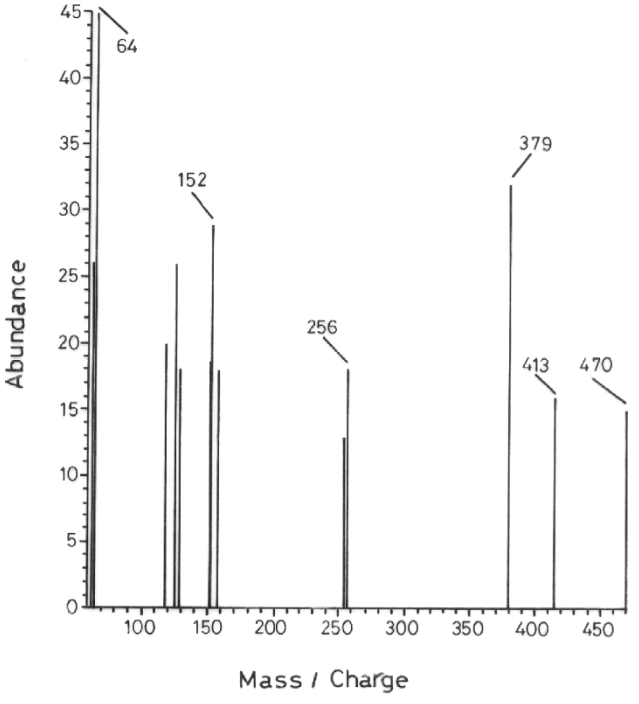

Figure 3. Mass spectrum of [Cu(A*p*ClPT)(OAc)(C_2H_5OH)] (**4**).

3.4. *Mass spectra*

The mass spectra for most of the complexes and the molecular ion peaks confirmed the proposed formulae. Calculated and found molecular weights are given in table 2. As a typical example, the mass spectrum (figure 3) of [Cu(A*p*ClPT)(OAc)(C_2H_5OH)] (**4**) shows peaks corresponding to the successive degradation of the molecule. The first peak at *m*/*e* 470 (Calcd. 471) represents the molecular ion peak of the complex (M^{+1}) with 33.33% abundance. The sharp peak (base peak) with *m*/*e* 64 represents the stable and final residue (Cu). Scheme 1 demonstrates the proposed degradation steps for the investigated complex.

3.5. *ESR spectra*

The spin Hamiltonian parameters and the *G* values of some of the solid Cu(II) complexes ($S=1/2$, $I=3/2$) are given in table 5. The ESR spectra of the complexes are quite similar and display axially symmetric *g*-tensor parameters with $g_{\|} > g_{\perp} > 2.0023$ indicating that the copper site has a $d_{x^2-y^2}$ ground state, characteristic of square-planar or octahedral geometry [30].

In axial symmetry, the *g*-values are related to the *G*-factor by the expression, $G=(g_{\|}-2)/(g_{\perp}-2)$. According to Hathaway [31], if the value of *G* is greater than 4, the exchange interaction between copper(II) centers in the solid state is negligible, whereas when it is less than 4, a considerable exchange interaction exists in the solid complex. Analysis of the ESR spectrum of the complex

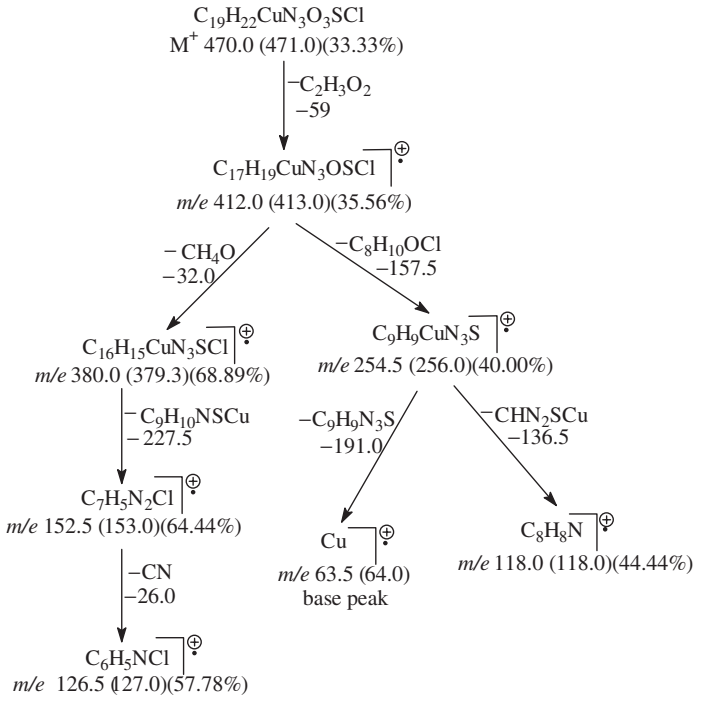

Scheme 1. Fragmentation pattern of [Cu(A*p*ClPT)(OAc)(C_2H_5OH)] (**4**).

[Cu(AT)(OH)(H_2O)$_3$] (**1**) indicates that $g_\parallel > g_\perp > 2.0023$ and $A_\parallel = 170 \times 10^{-4}\,cm^{-1}$. This observation suggests an elongated octahedral geometry [31]. The powder ESR spectral profile of [Cu_2(APT)$_3$(OAc)] (**3**) is typical of square-planar copper(II) and agrees well with the reported data [32, 33]. Also, the spectrum showed an additional weak ESR absorption at ~ 1500 G near $g = 4$ for a spin-coupled Cu(II) dimer which is not observed in the other two complexes (table 4). The small $g_\parallel$ values indicate strong interaction between the ligand and the metal ion. The ESR spectrum of [Cu(HST)$_2$]·H_2O (**5**) reveals that the Cu(II) center is axial with simulated spin Hamiltonian parameters $g_\parallel = 2.27$, $g_\perp = 2.08$ and $A_\parallel = 160 \times 10^{-4}\,cm^{-1}$. These values are most closely correlated with copper(II) ions with a tetrahedral structure ($g_\parallel = 2.25$ and $A_\parallel \approx (150\text{–}250) \times 10^{-4}\,cm^{-1}$ [34]. The G factor in [Cu(AT)(OH)(H_2O)$_3$] (**1**) is higher than 4 suggesting the absence of exchange coupling between copper(II) centers in the solid state [30], while in [Cu_2(APT)$_3$(OAc)] (**3**) and [Cu(HST)$_2$]·H_2O (**5**), G is less than 4 suggesting copper–copper exchange interactions.

The molecular-orbital coefficients, α^2 (a measure of the covalency of the in-plane σ-bonding between the 3d orbital and the ligand orbitals) and β^2 (the covalent in-plane π-bonding) were calculated employing the following equations [35]:

$$\alpha^2 = -(A_\parallel/0.036) = (g_\parallel - 2.0023) + 3/7(g_\perp - 2.0023) + 0.04$$
$$\beta^2 = (g_\parallel - 2.0023)E/ - 8\lambda\alpha^2,$$

where $\lambda = -828\,cm^{-1}$ for the free copper(II) ion and E is the electronic transition energy. The lower value of α^2 compared to β^2 indicates that the σ-bonding in plane is more covalent than the in-plane π-bonding. These data are in good agreement with the data reported earlier [31, 35]. The α^2 value (0.91) in the complex $[Cu(HST)_2]\cdot H_2O$ (**5**) indicates the existence of slight ionic character for the metal–ligand σ-bonding, where the value of β^2 (0.89) indicates the presence of considerable contribution of metal–ligand π-bonding in the plane.

3.6. *Thermal studies*

Non-isothermal calculations have been extensively used to evaluate the kinetic and thermodynamic parameters for the different thermal decomposition steps in the complexes employing the Coats–Redfern [36] and the Horowitz–Metzger [37] equations. Activation enthalpies ($\Delta H^{\#} = E - RT$), activation entropies ($\Delta S^{*} = 2.303$ [log (Zh/KT)]R) and free energies of activation ($\Delta G^{\#} = \Delta H^{\#} - T\Delta S^{\#}$) are given in table 6, where Z, K and h are the pre-exponential factor, Boltzman and Plank constants, respectively [38]. The kinetic parameters calculated by the Horowitz–Metzger method revealed no significant difference from those evaluated by the Coats–Redfern method. The activation energies could not be calculated for unsuitable or overlapped steps. The high value of E for the complex $[Cu(HSPT)(OAc)(H_2O)_2]\cdot H_2O$ (**7**) indicates that the ligand is strongly bonded to the Cu(II) ion. The E value observed for the second decomposition stage of $[Cu(AT)(OH)(H_2O)_3]$ (**1**) was found to be higher than that of the first indicating a low rate of decomposition. In the complex $[Cu(HSPT)(OAc)(H_2O)_2]\cdot H_2O$ (**7**), the E value for the second step is lower than that of the first one explaining why its rate of decomposition is high [12]. During the decomposition reactions, a reverse effect was observed where the rate of removal of the remaining ligand was smaller after the expulsion of one or two ligands except for $[Cu(AT)(OH)(H_2O)_3]$ (**1**).

The negative $\Delta S^{\#}$ values for all decomposition steps in all complexes indicate that the complexes, with the exception of $[Cu(HSPT)(OAc)(H_2O)_2]\cdot H_2O$ (**7**), are more ordered [39]. The activation energy of the first step (table 6) shows the following sequence: $[Cu(HSPT)(OAc)(H_2O)_2]\cdot H_2O$ (7) > $[Cu_2(APT)_3(OAc)]$ (**3**) > [Cu(A*p*ClPT)-(OAc)(C_2H_5OH)] (**4**) > $[Cu_2(BT)(OAc)(OH)_2(H_2O)]\cdot H_2O$ (**11**) > $[Cu(AT)(OH)\text{-}(H_2O)_3]$ (**1**).

In the thermograms (30–1000°C) of some complexes, the first step corresponds to the evolution of water of crystallization and/or coordinated water and the end products may be CuS, CuO or Cu.

The thermogram (figure 4) of the complex $[Cu_2(SpClPT)(OH)_2(H_2O)_2]$ (**8**) is taken as a representative example for the decomposition of these complexes. It is characterized by four degradation steps in the range 188–234, 234–269, 498–673 and 673–877°C (scheme 2). Elimination of two H_2O and two OH (Calcd. 13.9%, found 14.5%) is the first step. The second step consumes a C_6H_4O radical (Calcd. 18.4%, found 19.0%). The first, second and fourth steps are not suitable for kinetic analysis. The third step is slow with an activation energy of $107.2\,kJ\,mol^{-1}$ (Coats–Redfern eqn.) and first order. The radical C_6H_4Cl is assumed to be evolved in the third and fourth steps (Calcd. 22.6%, found 23.3%). Moreover, the thermogram shows a progressive decomposition up to 900°C after which a constant weight was observed and the (CuS + Cu) product (Calcd. 31.7%, found 30.6%) was the final residue.

Table 6. Kinetic and thermodynamic parameters for the thermal decomposition of some of the complexes.*

		Coats–Redfern eqn.			Horowitz–Metzger eqn.					
Compound	Step	r	n	E	r	n	E	$\rho S^{\#}$	$\rho H^{\#}$	$\rho G^{\#}$
$[Cu(AT)(OH)(H_2O)_3]$ (**1**)	1st	0.9917	0.33	36.0	0.9959	0.33	43.6	−268.5	32.1	157.5
	3rd	1.0000	2.00	91.6	0.9995	2.00	101.7	−206.3	86.0	224.2
$[Cu(AET)(OH)(H_2O)]$ (**2**)	2nd	1.0000	2.00	73.8	0.9995	2.00	84.2	−172.4	70.0	148.9
	4th	0.9999	0.66	267.1	0.9998	0.66	282.7	−56.5	259.3	312.6
$[Cu_2(APT)_3(OAc)]$ (**3**)	1st	0.9950	1.00	92.6	0.9932	1.00	100.7	−149.7	88.6	159.5
$[Cu(ApClPT)(OAc)(C_2H_5OH)]$ (**4**)	1st	0.9948	1.00	59.9	0.9939	1.00	65.3	−226.1	55.9	162.4
$[Cu(HSPT)(OAc)(H_2O)_2]\cdot H_2O$ (**7**)	1st	0.9988	2.00	373.3	0.9984	2.00	374.9	391.4	368.9	163.8
	2nd	1.0000	2.00	275.3	0.9999	2.00	285.3	−16.8	268.6	266.6
$[Cu_2(SpClPT)(OH)_2(H_2O)_2]$ (**8**)	3rd	0.9944	1.00	107.2	0.9940	1.00	117.4	−233.8	100.1	299.1
$[Cu_2(BT)(OAc)(OH)_2(H_2O)]\cdot H_2O$ (**11**)	1st	0.9941	1.00	39.0	0.9931	1.00	42.8	−274.0	34.9	169.4
	2nd	1.0000	0.33	73.4	0.9999	0.33	87.7	−242.8	67.7	234.0

*r = Correlation coefficient, n = order of the decomposition reaction; E, $\rho H^{\#}$ and $\rho G^{\#}$ are in kJ mol^{-1}, $\rho S^{\#}$ in JK mol^{-1}.

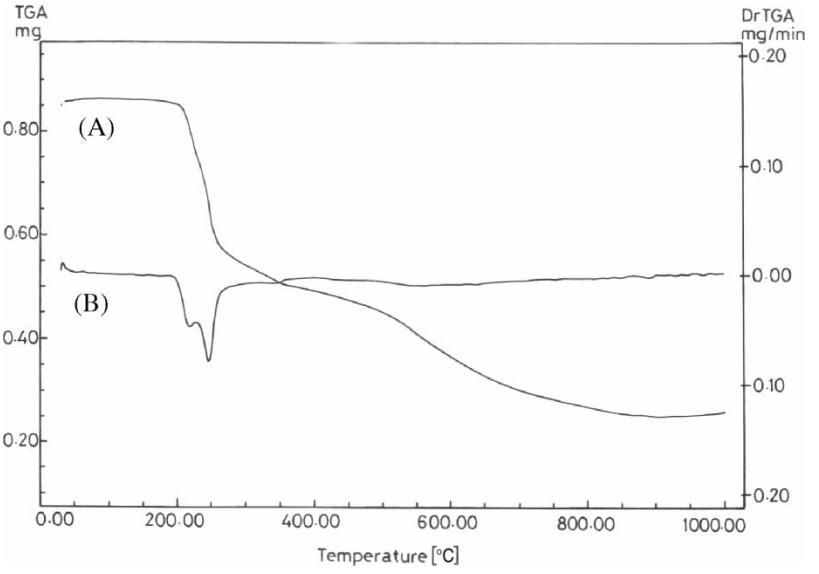

Figure 4. TG (A) and DTG (B) thermograms of $[Cu_2(SpClPT)(OH)_2(H_2O)_2]$ (**8**).

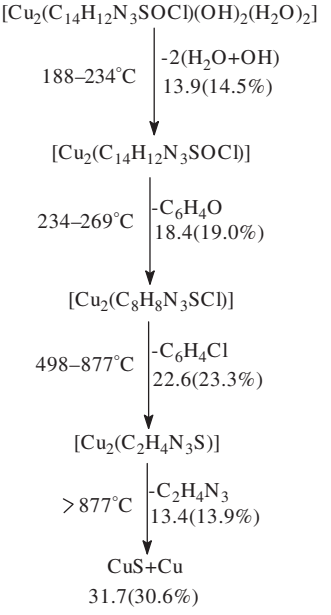

Scheme 2. Proposed thermal decomposition pattern of $[Cu_2(SpClPT)(OH)_2(H_2O)_2]$ (**8**).

3.7. *Redox properties*

Electrochemical responses of the mononuclear complexes (**1**), (**2**) and (**4**) were investigated in $DMF - TBA^+BF_4^-$ solutions by cyclic voltammetry at incremental scan rates (10–200 mV s^{-1}) *versus* Ag/AgCl reference electrode. The voltammetric data are summarized in table 7. The complexes showed similar features in the investigated

Table 7. Electrochemical data of some of the copper(II) complexes in DMF – $TBA^+BF_4^-$ *vs* Ag/AgCl at 100 V s^{-1}.*

	First electrode couple				Second electrode couple				Third electrode couple			
Complex	$E_{p,a}$	$E_{p,c}$	ΔE_p	$E_{1/2}$	$E_{p,a}$	$E_{p,c}$	ΔE_p	$E_{1/2}$	$E_{p,a}$	$E_{p,c}$	ΔE_p	$E_{1/2}$
$[Cu(AT)(OH)(H_2O)_3]$ (**1**)	−0.25	−0.60	0.35	−0.43	0.24	0.04	0.20	0.14	0.80	0.68	0.12	0.74
$[Cu(AET)(OH)(H_2O)]$ (**2**)	−0.26	−0.64	0.38	−0.45	0.17	0.05	0.12	0.11	0.78	0.68	0.10	0.73
$[Cu_2(APT)_3(OAc)]$ (**3**)	0.04	−0.36	0.40	−0.16	0.27	−0.05	0.32	0.11	0.81	0.69	0.12	0.75
$[Cu(A\textit{p}ClPT)(Oac)(C_2H_5OH)]$ (**4**)	−0.25	−0.56	0.31	−0.40	0.33	0.16	0.17	0.25	0.94	0.73	0.21	0.83

*$E_{1/2} = (E_{p,c} + E_{p,a})/2$.

potential range −1.2–1.4 V and displayed three well-defined reduction waves in the regions −0.64 to −0.36, 0.04–0.16 and 0.68–0.73 V coupled with three anodic waves in the regions −0.26–0.04, 0.17–0.33 and 0.78–0.94 V with $E_{1/2} = -0.40$ to 0.16; 0.11–0.25 and 0.73–0.83, respectively. Comparison with analogous copper(II) complexes [7, 40], for the nearly irreversible ($\Delta E_p \geq 0.1$ V) electrode couples allow assignment to one-electron oxidation processes Cu^0/Cu^I, Cu^I/Cu^{II} and Cu^{II}/Cu^{III}, respectively. The one-electron nature of these irreversible electrode couples has also been established by comparing its current height with similar couples displayed by analogous copper(II) complexes [40].

The electron-withdrawing (*p*-ClC_6H_4) group in the complex [Cu(A*p*ClPT)(OAc)(C_2H_5OH)] (**4**) shifts the oxidation potential of the electrode couples Cu^I/Cu^{II} and Cu^{II}/Cu^{III} to more positive values and makes their reduction processes more difficult compared with [Cu(AT)(OH)(H_2O)$_3$] (**1**) and [Cu(AET)(OH)(H_2O)] (**2**) (table 7). The electron-attracting *p*-ClC_6H_4 group lowers the electron density at the reduction center, which becomes more positive and more easily reduced. The presence of the C_2H_5 (electron-donating) group has an opposite effect to that

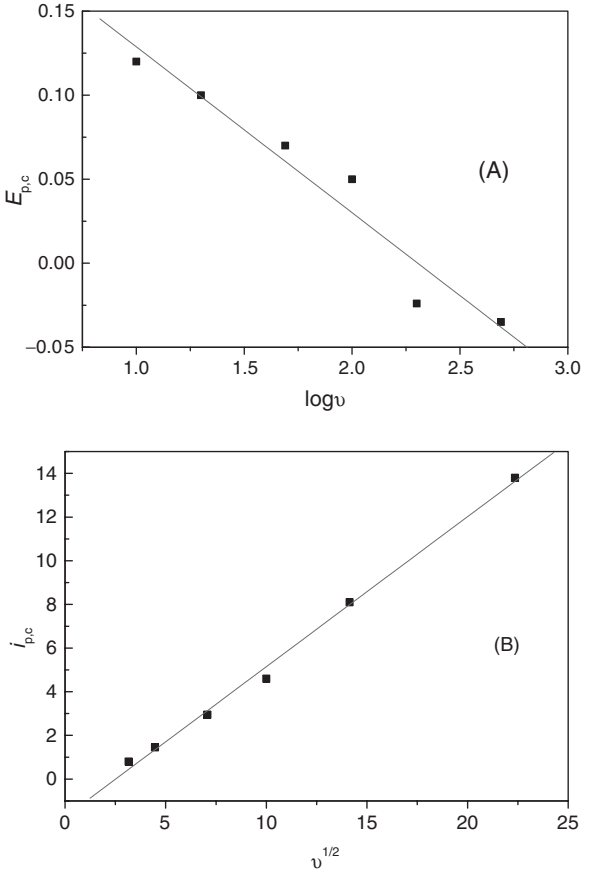

Figure 5. Dependence of the cathodic peak potential, $E_{p,c}$ (A) and the cathodic peak current, $I_{p,c}$ (B) on the scan rate of the electrode couple Cu^{III}/Cu^{II} of [Cu(AT)(OH)(H_2O)$_3$] (**1**).

reported for the reduction of similar compounds [5, 6]. The ethyl group makes both oxidation and reduction processes more difficult than for $[Cu(AT)(OH)(H_2O)_3]$ (**1**). This may be explained by the steric effect of the ethyl group at the reduction center, which would hinder the approach of the reduction center to the electrode surface [41].

The dependence of the cathodic peak current, $i_{p,c}$, of the electrode couple Cu^{III}/Cu^{II} on the square root of the sweep rate ($v^{1/2}$) for (**1**) suggests a diffusion-controlled electrochemical process [42] (figure 5). The cathodic peak potential ($E_{p,c}$) of this couple shifts towards more negative values as v increases indicating an irreversible electrode couple, which was also confirmed from the linear dependence of the cathodic peak potential, $E_{p,c}$, with log v [43] (figure 5). The product of the number of electrons involved in the reduction process (n) and the corresponding charge-transfer coefficient (α) can be determined from the slope of this line. Assuming $n = 1$, $\alpha = 0.62$, which is in the expected range for a single one-electron transfer step [42]. A similar feature was observed for the couples of H and NH_2 derivatives.

Characteristic cyclic voltammograms for (**1**) at −1.2–0.0 V are shown in figure 6. A slight displacement of the anodic and cathodic peaks is observed as the sweep rate increases, the peak current ratios $i_{p,c}/i_{p,a} > 1$; $\Delta E_p > 60$ mV and the $i_{p,c}$

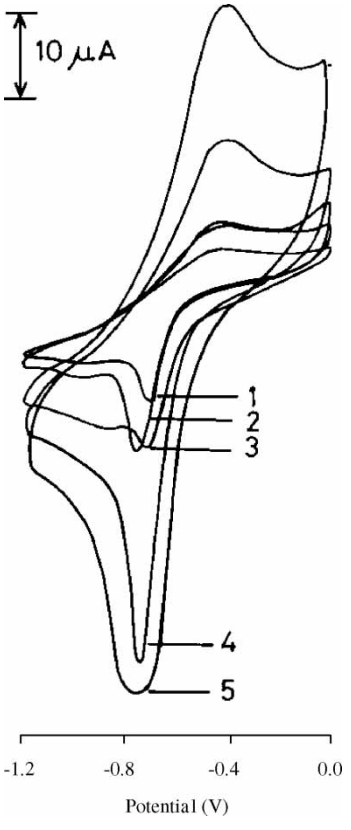

Figure 6. Influence of scan rate ($mV\,s^{-1}$) on the electrode couple Cu^{II}/Cu^{I} of $[Cu(AT)(OH)(H_2O)_3]$ (**1**). 10 (1), 20 (2), 50 (3), 100 (4) and 200 (5) $mV\,s^{-1}$.

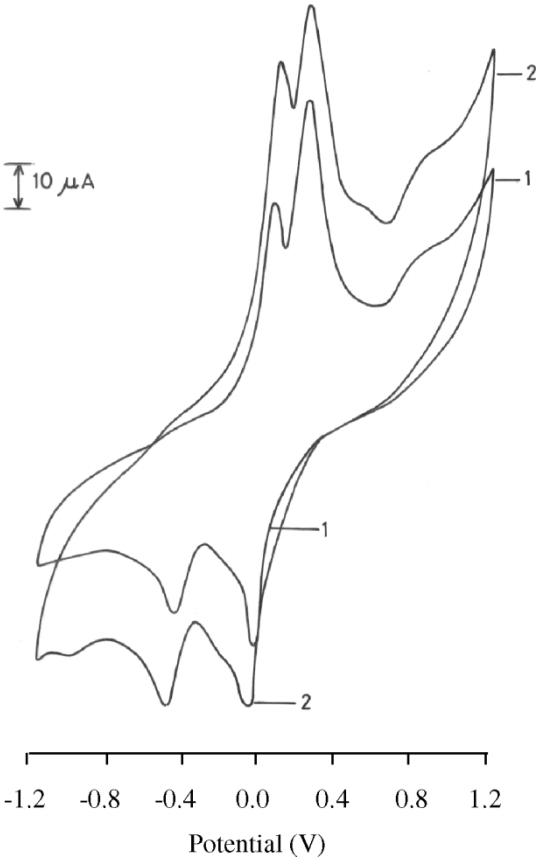

Figure 7. Cyclic voltammograms of $[Cu_2(APT)_3(OAc)]$ (**3**) at 100 (1) and at 200 (2) $mV\,s^{-1}$ in $DMF - TBA^+BF_4^-$ *vs* the Ag/AgCl reference electrode.

versus $\nu^{1/2}$ plot is linear with a positive intercept. All these characteristics indicate an irreversible, one-electron process. The dependence of the voltammetric response of Cu^I/Cu^0 on the sweep rate, the depolarizer concentration of the analyte as well as the decrease in $i_{p,c}/\nu^{1/2}$ is typical of an ECE (electrochemical reaction coupled between two charge processes) type mechanism in which an irreversible first-order chemical reaction is interposed between two successive one-electron charge transfers. The ECE mechanism of this complex was also confirmed by the observed decrease of cathodic peak current vs. the $\nu^{1/2}$ and from $i_{p,c}/\nu^{1/2} > 1$ on increasing the scan rate.

The CV of binuclear complex (**3**) at $100\,mV\,s^{-1}$ sweep rate is shown in figure 7 and summarized in table 7. The irreversible nature and the ECE-type mechanism of the observed reduction peaks were confirmed by the large difference in the potential ($\Delta E_p > 0.1\,V$) between the two peak centers of the couples Cu^I/Cu^0 and Cu^{II}/Cu^I and the linear dependence of the cathodic peak potential, $E_{p,c}$, of each electrode process with log ν. At $\nu \leq 200\,mV\,s^{-1}$ the CV showed two irreversible reduction peaks coupled with two irreversible oxidation waves in the potential range -1.2–$1.2\,V$. At the highest scan rate ($> 200\,mV\,s^{-1}$) such behavior is prevented.

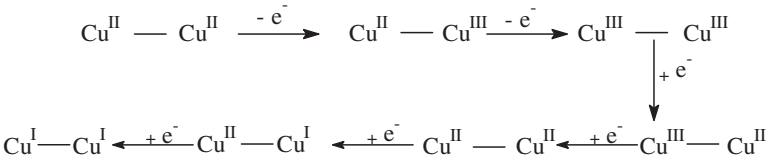

Scheme 3. Proposed electrochemical behavior of $[Cu_2(APT)_3(OAc)]$.

These observations may be attributed to the sequential one-electron transfer reactions as shown in scheme 3.

Similar sequential one-electron transfer for a number of binuclear Cu^{2+} complexes has been reported [44, 45]. These data confirm the proposed binuclear structure.

The $E_{1/2}$ values for the electrode couple Cu^I/Cu^0 of the mononuclear complexes are more negative compared with the binuclear complex. This difference may be due to the binuclear complex accepting an electron more easily due to electrostatic effects compared to mononuclear complexes. The ΔE_p of the Cu^I/Cu^0 couple for mononuclear complexes is also smaller than the binuclear one. This difference may be due to the binuclear Cu(II) complexes undergoing Cu–N or Cu–S bond rupture as soon as Cu^I reduces to Cu^0 [46].

References

[1] M. Abram, E.S. Lang, E. Bonfada, *Z. Anorg. Allg. Chem.*, **628**, 1419 (2002).
[2] R. Pogni, M.C. Baratto, A. Diaz, R. Basasi, *J. Inorg. Biochem.*, **79**, 333 (2000).
[3] M.B. Ferrari, F. Bisceglie, G. Pelosi, M. Sassi, P. Tarasconi, M. Cornia, S. Capacchi, R. Albertini, S. Pinelli, *J. Inorg. Biochem.*, **90**, 113 (2002).
[4] S.D. Dhumwad, K.B. Gudasi, T.R. Goudor, *Indian J. Chem.*, **33A**, 320 (1994).
[5] E. Franco, E. Lopez-Torres, M.A. Mendiola, M.T. Sevilla, *Polyhedron*, **19**, 441 (2000) and references therein.
[6] D.W. Maragerum, G.D. Owens, In *Metal Ions in Biological Systems*, H. Sigel (Ed.), Marcel Dekker, New York (1981).
[7] P. Bindu, M.R.P. Kurup, T.R. Salyakeerty, *Polyhedron*, **18**, 321 (1999).
[8] M.B. Ferrari, S. Capacchi, G. Pelosi, G. Reffo, P. Tarasconi, R. Albertini, S. Pinell, P. Lunghi, *Inorg. Chim. Acta*, **286**, 134 (1999).
[9] D.X. West, A.A. Nassar, F.A. El-Saied, M.A. Ayad, *Transition Met. Chem.*, **23**, 321 (1998).
[10] D.X. West, H. Gebremedhin, R.J. Butcher, J.P. Jasinski, A.E. Liberta, *Polyhedron*, **12**, 2489 (1993).
[11] R.M. El-Shazly, G.A.A. Al-Hazmi, S.E. Ghazy, M.S. El-Shahawi, A. El-Asmy, *Spectrochim. Acta A*, **60**, 3187 (2004).
[12] D.X. West, Y.-H. Yang, T.L. Klein, K.I. Goldberg, A.E. Liberta, J. Valdes-Matinez, S. Hernandez-Ortega, *Polyhedron*, **14**, 1681 (1995).
[13] S.I. Mostafa, A.A. El-Asmy, M.S. El-Shahawi, *Transition Met. Chem.*, **25**, 470 (2000).
[14] A.I. Vogel, *A Text Book of Quantitative Inorganic Analysis*, Longman, London (1972).
[15] H.M. Irving, H.S. Rossotti, *J. Chem. Soc.*, 2904 (1954).
[16] D.X. West, S.L. Dietrich, I. Thientanavanich, C.A. Brown, *Transition Met. Chem.*, **19**, 195 (1994).
[17] D.X. West, A.K. El-Sawaf, G.A. Bain, *Transition Met. Chem.*, **23**, 1 (1998).
[18] D.X. West, M.M. Salberg, G.A. Bain, A.E. Liberta, *Transition Met. Chem.*, **22**, 180 (1997).
[19] K. Nakamoto, *Infrared and Raman Spectra of Inorganic and Coordination Compounds*, 3rd Edn, p. 305, Wiley, New York (1978).
[20] A.H. Osman, A.A.M. Aly, N.A. El-Maali, G.A.A. Al-Hazmi, *Synth. React. Inorg. Met.-Org. Chem.*, **32**, 1293 (2002).
[21] A.H. Osman, A.A.M. Aly, N.A. El-Maali, G.A.A. Al-Hazmi, *Synth. React. Inorg. Met.-Org. Chem.*, **32**, 663 (2002).
[22] H. Iriving, H. Rossotti, *Acta Chem. Scand.*, **10**, 72 (2002).
[23] A.A. El-Asmy, M.E. Khalifa, M.M. Hassanian, *Synth. React. Inorg. Met.-Org. Chem.*, **31**, 1787 (2001).

[24] L.M. Fostak, I. García, J.K. Swearingen, E. Bermejo, A. Castiñeiras, D.X. West, *Polyhedron*, **22**, 83 (2003).
[25] S. Mostafa, M.M. Bekheit, M.M. El-Agez, *Synth. React. Inorg. Met.-Org. Chem.*, **30**, 2029 (2000).
[26] A. Sreekan, M.R.P. Kurup, *Polyhedron*, **22**, 3321 (2003).
[27] D.X. West, M.A. Lockwood, M.D. Owens, A.E. Liberta, *Transition Met. Chem.*, **22**, 366 (1997).
[28] R.M. El-Shazly, A.A. El-Asmy, A. El-Shekeil, *Synth. React. Inorg. Met. -Org. Chem.*, **21**, 385 (1991).
[29] N.T. Akinchan, D.X. West, Y.H. Yang, M.M. Salberg, T.L. Klein, *Transition Met. Chem.*, **20**, 481 (1995).
[30] G. Speie, J. Csihony, A.M. Whalen, C.G. Pie-Pont, *Inorg. Chem.*, **35**, 3519 (1996).
[31] B.J. Hathaway, *Struct. Bonding* (*Berlin*), **57**, 55 (1984).
[32] M.L. Miller, S.A. Ibrahim, M.L. Golden, M.Y. Daresbourg, *Inorg. Chem.*, **42**, 2999 (2003).
[33] A. Diaz, A. Fragosa, R. Cao, V. Vérez, *J. Carbohydrate Chem.*, **17**, 293 (1998).
[34] P. Comba, T.W. Hambley, M.A. Hitchman, H. Stratemeier, *Inorg. Chem.*, **34**, 3903 (1995).
[35] K. Jayasubramanian, S.A. Samath, S. Thambidurai, R. Murugesan, S.K. Ramalingam, *Transition Met. Chem.*, **20**, 76 (1995).
[36] A.W. Coats, J.P. Redfern, *Nature*, **20**, 68 (1964).
[37] H.H. Horowitz, G. Metzger, *Anal. Chem.*, **25**, 1464 (1963).
[38] R.M. Mahfouz, M.A. Monshi, S.M. Alshehri, N.A. El-Salam, A.M.A. Zaid, *Synth. React. Inorg. Met.-Org. Chem.*, **31**, 1873 (2001).
[39] A.A. Aly, A.S.A. Zidan, A.I. El-Said, *J. Thermal Analysis*, **37**, 627 (1991).
[40] E. Franco, E. Lopez-Torres, M.A. Mendiole, M.T. Sevilla, *Polyhedron*, **19**, 441 (2000).
[41] G.M. Abdou-Elenien, N.A. Ismail, M.M. Hassanin, A.A. Fahmy, *Can. J. Chem.*, **70**, 2704 (1992) and references therein.
[42] L.M. Araya, J.A. Vargos, J.A. Costamana, *Transition Met. Chem.*, **11**, 312 (1986).
[43] B.S. Parajon-Costa, A.C. Gonzalez-Baro, E.J. Baran, *Z. Anorg. Allg. Chem.*, **628**, 1628 (2002).
[44] B. Adhikary, S.K. Mandal, K. Nag, *J. Chem. Soc. Dalton Trans.*, 935 (1988).
[45] R.C. Long, D.N. Hendrickson, *J. Am. Chem. Soc.*, **105**, 1513 (1983).
[46] C. Parter, *Coord. Chem.*, **28**, 297 (1997).